# SCIENTIFIC REP aRTS

# **OPEN**

# Layer-by-Layer Insight into Electrostatic Charge Distribution of Few-Layer Graphene

Rece ived:09 November 2016 Accepted:16 January 2017 Published: 21 February 2017

Hossein Rokni &Wei Lu

In few-layer graphene (FLG) systems on a dielectric substrate such as SiO<sub>2</sub>, the addition of each extra layer of graphene can drastically alter their electronic and structural properties. Here, we map the chargedistribution among the individual layers of finite-size FLG systems using a novel spatial discrete model that describes both electrostatic interlayers creening and fringefield effects. Our results reveal that the charge density in the region very close to the edges is screened out an order of magnitude more weakly than that across the central region of the layers. Our discrete model suggests that the interlayer charge screening length in 1-8 layer thick graphenesystems depends mostly on the overall gate/molecular doping level rather than on temperature, in particular at an induced charge density  $> 5 \times 10^{12} \, \mathrm{cm}^{-2}$ , and can reliably be determined to be larger than half the interlayer spacing but shorter than the bilayer thickness. Our model can be used for designing FLG-based devices, and offers a simple rule regarding the charge distribution in FLG: a pproximately 70%, 20%, 6% and 3%(99% overall) of the total induced charge density reside within the four in nermost layers, implying that the gate-induced electric field is not definitely felt by > 4th layer.

Since its discovery in 2004, single-layer graphene (SLG) has become the most studied nanomaterial due to its exceptional mechanical<sup>1</sup> electrical2 and opticaP properties. Although several physical properties are shared between SLG and few-layer graphene (FLG), increasing layer thickness can give rise to a unique range of electronic and structural properties that has not yet been sufficiently understood, in particular for FLG systems with more than 3 layers. More specifically, electrical noise, charge transport and nonlinear optical properties of FLG on substrates (usuallySiOifSi) exhibit strongdependence on the number oflayers, gate-induced chargedensities and underlying oxide substrates. It is therefore crucial in the design of FLG-based high-speed transistors<sup>4</sup> terahertz plasmonics<sup>5</sup>, photonicsand optoelectronicdevices6 to quant itatively understand the role of the number of layers in the charge distribution and the electric field screening of the FLG/SiOifSi systems and also to explore the unclear relationship between the excess gate-ind uced chargedensities and the layer-by-layer Fermi level and charge density profiles in the FLG systems.

Owing to the importance of the subject, the question of interlayer charge screening length >.. in the FLG systems has been addressed by several exper imental methods, including angle-resolved photoemission spectroscopy (>..= 0. 1 4 - 0 . 19 nm)7, no ndegenerate ultrafast mid-infrared pump-probe spectroscopy (>..= 0.34nm)8. Kelvin probe force microscopy9· <sup>13</sup> (>..= 1.36 - 1.70 nm <sup>11</sup>,>..= 0 . 42 nm <sup>12</sup> and >..= 2.4 nm <sup>13</sup>), single gated field effect transistor (>..= 0.6 nm) 14, doub le-ga ted fie ld effect transistor (>..= 1.2 nm) 15 and dark -fie ld sc atte ring spec troscop y  $(>..=1.2\pm0.2~{\rm nm})^{16}~{\rm However}$ , a relatively wide range of experimental values for>.. (from less than a single layer to seven layers) is observed, which is not yet fully understood. Nevertheless, we believe that a part of this data scattering maybe attributed to the dependence of the screening length on the device quality and experimental conditions, such as sample preparation processes, the presence of defects and impurities in graphene, the intrinsic charge density in each graphene layer and the actual doping level of the system. This diversity in the reported values of >.. is also seen in theoretical approaches 1,720 Depending on whether the inter-layer electron tunneling is taken into account or not, >.. between 0.54 nm<sup>17</sup> and 0.7 nm<sup>18</sup> is obtained using a random phase approximation. Kuroda and coworkers theoretically reported that both the gate charge and temperature could highly influence >., whose value may range from ~0.2nm to 3.1nm. 9. We will later show in this paper that the presence of the effective mass, a key missing param eter in Kuroda's model'.9 not onlyleadsto a much narrower range of>..values (= 0.2 - 0.7 nm), but also rules out the possible effect of temperature on the reported values of \( \)... We also note

Department of Mecha nical Engineering, University of Michigan, Ann Arbor, Michigan 48109, United States. Correspondence and requests for materials should be addressed to W.L. (em a il: weilu@umich.edu)

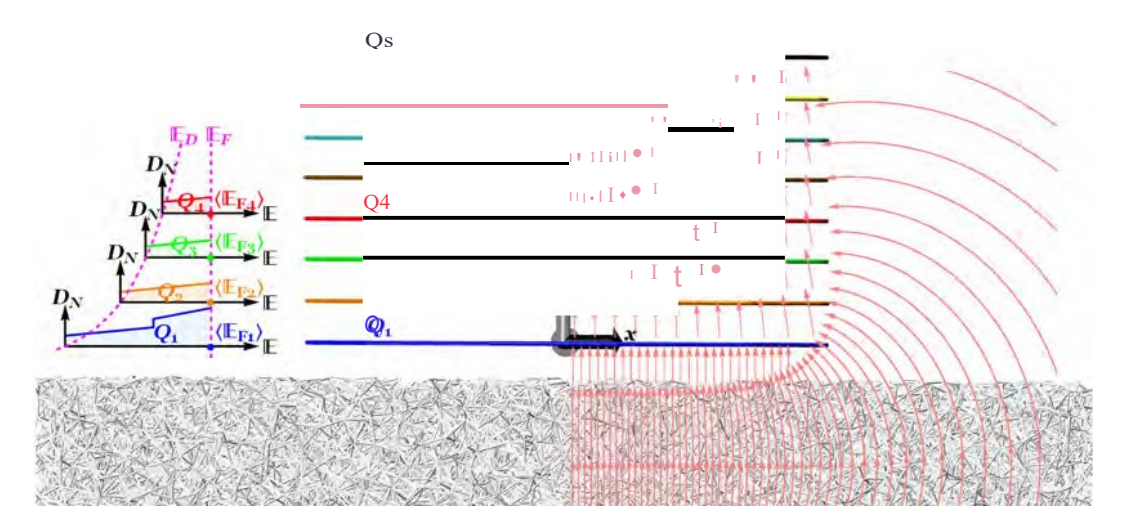


Figure I. Schematic illustration of an eight-layergraphene/SiO $_2$  system. The Sisubstrate beneath the SiO $_2$  film is not shown for simplicity. The arrows correspond to the electric field linesfocusing near the edges of FLG. Left inset: density of states in the four innermost graphene flakes versus the electronic band energy, where the transparent area represents the average induced chargedensity Q; and the average value of the Fermi energy profile is denoted by(EF;).

that the >.. value of 2.4nm reported in ref. 13 was extracted from Kuroda's model, while our discrete model yields a value of 0.33nm.

Finite-size FLG flakes and graphene nanoribbons in actual devices exhibit an intriguing dependence of the electrostatic and electrical conductivity response on their geometrical parameters (e.g., lateral sizes, thicknesses, shapes and edge types)<sup>21</sup>.2<sup>2</sup>. Both experimental and theoretical studies have demonstrated that a strong charge accumulation takes place at the edges of the finite-size graphene flake due to the electrostatic fringe field effects<sup>2</sup>>-3.¹ Scanning gate microscope measurements of a monolayer graphenedeviceon a SiOifSi substrate reveal significant conductance enhancement at the edge of the graphene device due to the strong charge accumulation<sup>23</sup> Similar observations of inhomogeneous chargedensity and capacitance profiles near the edges of bothsuspended and hBN-supported mono/bilayergraphene devices have been reported using quantum Hall edge channels<sup>24</sup>.2<sup>5</sup> Among different theoretical models on the charge distribution of the finite-sized graphene, we particularly note a strong charge accumulation at the edges and the corners of a positively charged rectangular graphene sheet using the charge/dipole molecular dynamics modeJ2<sup>6</sup>.2<sup>7</sup> and along the edges of a graphene nanoribbon using the tight-binding modeJ2<sup>8</sup>

Despite recent progress, a detailed understanding of the electrostatic charge distribution in connection with the actual electronic structure of FLG is still lacking. Here, we exploit the layered nature of FLG to develop a novel spatial discrete model that successfulyl accounts for both electrostatic screening and fringe field effects on the charge distribution of the finite-size FLG system. To this end, an effective bilayer model based on two tight-binding parameters is utilized to accurately describe electronic band structures and thus density of states (DOS) of one to eight Bern al-stacked graphene layers. We then explore the unclear relationship between the gate-induced charge densities and layer-by-layer Fermi level and charge density profiles in FLG systems usin g a global energy minimization, where its total energy is calculated based on electrostatic interaction between graphene layers and band-filling energy in each layer. Our discrete model offers a unique capability to quantify the nonlinear charge density profile, interlayer capacitance, quantum capacitance, and local surface electrostatic potential of FLG by showing a verygoodqualitative and quantitative agreement between the previously measured work functions in FLG and our theoretical results.

## Spatial Discret e Mo del

We first examine the charge distribution of an FLG/SiOifSi system containing N (up to 8) layers of finite-size graphene sheet with desired shapes (i.e., square, rectangle, circle or ribbon), as schematically illustrated in Fig. 1(a). Each graphene layer is labeled by an integer number starting from i = 1 for the layer closet to the substrate (hereafter referred to as the innermost layer) to i = N for the top layer (as the outermost layer). Applying a biasvoltage  $V_0$  between the highly-doped Si substrate and N-layer graphene (N-LG) induces a total excess charge density of  $Q_0$  in N-LG, whose layer i can carry a charge density of  $Q_1$  such that the following constraint holds  $Q_0 = I$ : f: f:

The electronic bands of N-LGcan be modeled by two tight-binding parameters, namely, the nearest neighbor hopping parameter  $_{10}$  (which defines the Fermi velocity  $_{y=}$  ( $_{3l}$   $_{2}$ ) $_{10}$   $_{2}$   $_{3}$   $_{4}$   $_{8}$ , where  $_{2}$  = 0.142  $_{8}$   $_{8}$  is the C-C bond length) and the nearest neighbor interlayer coupling constant  $_{1}$ . We take  $_{10}$  = 3.14  $_{8}$   $_{8}$   $_{11}$  = 0.4 $_{8}$   $_{8}$   $_{11}$  values of bulk graphite. The energy dispersion in Bernal-stacked N-LG, obtained from 2D cuts in the electronic dispersion of graphite, perpendicular to the graphene planes at specific values of ( $_{10}$ = $_{10}$ - $_{10}$ ) can be given by  $_{10}$  =  $_{10}$   $_{1$ 

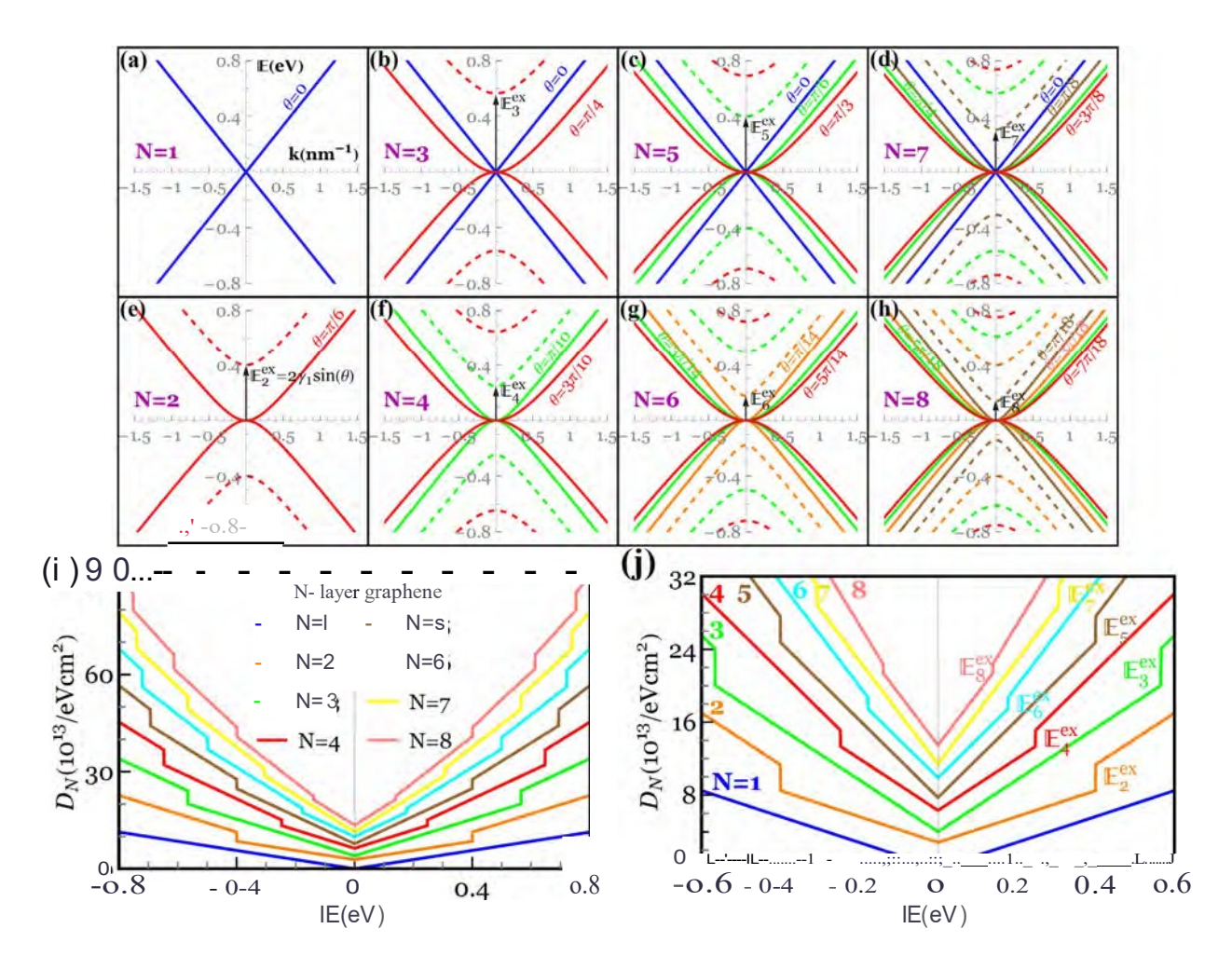


Figure 2. (a-h) Low-energy band structures of Bernal-stacked N-LG near the K-point of the Brillouin zone. Thereexist LN/2J pairs of split-off hyperbolic bands, where LJ denotes the integer part of the quantity. The excitation energy from the ground state to the first excited state (IE";) is shown with arrows. Blue lines in (a-d) correspond to the electronic dispersion of the effective monolayer graphene (0=0) which only appears in systems with an odd number of graphene layers, whereas red, green, pink and brown in (e-h) correspond to the electronic dispersion of the bilayer-like graphene (0=0). Negative and positive IE refer to the valence(hole)/conduction(electron) bands, respectively. (i) Density of states in N-LG showing discontinuous jumps at the excited states. (j) Zoom-in viewof discontinuous jumps at the first excited state (IE";).

kinetic energylE. Figure 2(a) through (h) illustrate low-energy band structures of N-LG (near the K-point of the Brillouin zone) up to N=8. It is seen that monolayer graphene (Fig. 2(a)) exhibits a well-known linear dispersion which results in massless excitations, whereas bilayer graphene (Fig. 2(e)) displays a set of four hyperbolic bands (with no Dirac electrons) touching at the so-called Dirac point. Though the band structure of trilayergraphene (Fig. 2(b)) comprises one pairoflinear (monolayer-like)bands and two pairs of hyperbolic (bilayer-like) bands, tetralayer graphene (Fig. 2(f)) interestinglyshows only four pairsof hyperbolic (bilayer-like) bands. In general, based on the tight-binding model described above, both monolayer and bilayer-like bands are present in odd multilayers (N?\_3), whereas the band structure of even multilayers only consists of the bilayer-like bands. Figure 2(a-h) confirm that N-LG should be considered a single 2D system (mj += 0), rath er than a composite system consisting of N parallel single layers of graphene with the linear energy dispersion (m += 0), as ex perimentally confirmed by micro magneto-Raman scattering spectroscopy in 1- to 5-LG sjstems magneto-Raman scattering spectroscopy in 1- to 5-LG sjstems magneto-Raman scattering spectroscopy dispersion model.

The density of states (DOS) in N-LG is obtained from the summation of the DOS for each energy band with double spin and double valley degeneracies

$$D_N(\mathbb{E}) = \sum_{l=1}^{N_b} \sum_j \frac{d}{d\mathbb{E}} \left( \frac{k_j^2}{\pi} \right) = \frac{2}{\pi \gamma^2} \sum_{l=1}^{N_b} \sum_j \left[ \mathbb{E} \pm \gamma_1 \sin \left( \frac{j\pi}{2(N+1)} \right) \right]$$
(1)

where Nb (= N/2 and (N + 1)/2 for even and odd multilayers, respectively) is the number of bands in IE and j= 21-1 and 2(/-1) for even and odd multilayers, respectively. A systematic evolution of Dv (JE) as a function of

the layer number in Fig. 2(i) reveals finite discontinuities at the split-off (excitation) energies Eex = 21 Isin 0) which are produced by the band extrema at the K-point, followed by a linear increase with kinetic energy IE. Of particular importance for the electronic structures of N-LGat low energies is the excitation energy from the ground state (Diracpoint) to the first excited state (denoted by JE), as explicitly shown in Fig. 20).

We next determine the charge distribution profile in a finite-size N-LG stack with a circular shape of radius *R*, based on the method of images, followed by solving the Love equation (Section S1.1 of Supplemental Material (SM)). The charged ensity profile in the circular layer *i* can then be expressed by

$$q_{i}(\mathbf{r}, \alpha_{i}, Q_{i}) = \frac{f(\mathbf{r}, \alpha_{i})}{\langle f \rangle} Q_{i}$$
(2)

where

$$f(\text{rr}, a;) = \underbrace{g(\text{rr})}_{J \le 1} Q.$$

$$\underbrace{J \le 1}_{0;} + \underbrace{0;}_{0} - \underbrace{\text{lf}}^{"}2^{-1}$$
(3)

is the charge distribution profile, normalized to its average value (j) for generality purposes; the index notation i varies from 1 to N;  $I^{n}$  (= r!R) is a dimension less parame ter; r denotes the radial coordinate of atom and g ( $I^{n}$ ) is a polynomial function of R which onlydepends on the ratio of the graphene size to the dielectric thickness (Fig. Sl of SM). A new parameter  $a_{1}$  (>0) is introduced by Eq. (3) in order to determine the amount of charge density at the edge of the layer i ( $I^{n}$  = 1). Although the focus of the present work is on graphene flakes with a circular shape, we note that the charge distribution of circular graphene flakes and graphene nanoribbons is of a similar form as given by Eq. (3) and, therefore, does not qualitatively and pretty much quantitatively alter the main results of this paper (Section Sl.2ofSM). We also refer the interested reader to Section Sl.3ofSM for the corresponding charge distribution profile of rectangular/square graphene flakes.

As we already discussed, in practice, the charge distribution in electrostatically doped graphene devices is inhomogeneous, yielding a non-uniform Fermi level profile. For instance, scanning gate microscope measurements of a monolayer graphene deviceon a SiOz/Si substrate reveals strongshift of the local Dirac point from the Fermilevel at the grapheneedge due to the contribution of both localized edgestates (i.e., zigzag or armchair) and accumulated charge along the edge<sup>2,3</sup> The Fermi energy profile eF; across the layer *i* can be expressed in terms of the constant Fermi energy eF, as follows (Section S2 of SM)

$$\mathbb{E}_{\mathrm{F}i}(\mathbf{r}, \alpha_i, \mathbf{e}_{\mathrm{F}i}) = -\frac{\gamma_1}{N_b} \sum_{l=1}^{N_b} \sum_{j} \sin \theta + \sqrt{\frac{f(\mathbf{r}, \alpha_i)}{\langle f \rangle N_b} \sum_{l=1}^{N_b} \sum_{j} (\mathbf{e}_{\mathrm{F}i}^2 + 2\mathbf{e}_{\mathrm{F}i} \gamma_1 \sin \theta) + \left[ \frac{\gamma_1}{N_b} \sum_{l=1}^{N_b} \sum_{j} \sin \theta \right]^2}$$

$$(4)$$

Then, the average chargedensity of each layer can be expressed by

$$Q_{1} = -\frac{eL \text{ {EF,}}}{N \text{ o}} DN(1E)d1E = -\frac{e \text{ Nb}}{2} \frac{2}{1: \text{ I: }} ((1E;) + 2(EF_{-1})7 \text{ sm0})$$

$$1r7 N_{1-1j}$$
(5)

where (IEFi) is the average value of IEFi in terms of IE; and  $a_1$  The average charge density Q, can be obtained by minimizing the total energy of the system with respect to eF; and  $a_1$  as the variational parameters under the constraint that  $Q_0 = I$ ;  $Z_{y_1}$  Q. In the N-LG/SiO; JSi system, the total energy can be split as,  $U_1 = U_1 + U_2 + U_3 + U_4 + U_4 + U_5 + U_$ 

$$U_{i} = -\frac{d}{2} \prod_{E \in [1-1]}^{N} Q_{0} - L Q_{i-1}^{2}$$

$$(6)$$

and

$$U_b = \frac{1}{N} \sum_{i=1}^{N} \int_{0}^{\langle \mathbb{E}_{\mathrm{F}i} \rangle} \mathbb{E} D_N(\mathbb{E}) d\mathbb{E} = \frac{1}{\pi \gamma^2 N} \sum_{i=1}^{N} \sum_{l=1}^{N} \sum_{i=1}^{N} \left[ \frac{2}{3} \langle \mathbb{E}_{\mathrm{F}i} \rangle^3 + \langle \mathbb{E}_{\mathrm{F}i} \rangle^2 \gamma_1 \sin \theta \right]$$
(7)

where *dis* the interlayer distance and *c*: is the dielectric constant in N-LG. For our numerical calculations, we use the value£= 1, which describes the N-LGsystem in vacuum. One may find the equivalent bias voltage applied between the Si substrate and N-LG by taking the derivative of the total energy with respect to the total induced

Figure 3. (a) Work functions across a 4-LGsystem which are given relative to that of the outermost layercl><sub>4</sub> as the zero -reference level for  $Q_0 = 2.2 \times 10^{13}$  cm  $^{-2}$ 7; (b) work functions in the 1-6-LGsystems relative to that of bulk graphite  $\Phi_{00}$  for  $Q_0 = 4.85 \times 10^{12}$  cm  $^{-21}$ 1; and (c) difference between the work function of the uppermost layer in the N-LGsystem and that in the (N-1)-LGsystem for N= 1 to 8 when  $Q_0 = 1.7 \times 10^{13}$  cm  $^{-212}$ 

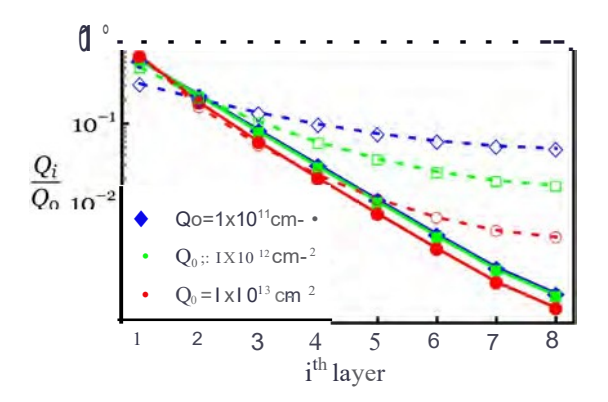


Figure 4. Normalized charge distribution profiles of an 8-LG system for three different values of  $Q_0$ . Dashed curves with open symbols represent the results obtained by the linear energy dispersion (mj = 0), whereas solid curves with filled symbols denote the results obtained by the actual energy dispersion of an 8-LG system (mj ,;, o 0).

charge density (i.e.,  $V_0 = dU, ldQ_0$ ) and local surface electrostatic potential of each layer can be obtained by  $V_i = dUJdQ_0$ .

### Re s ult s a nd Disc u ss io n

**C** o m p ari son Stud ies. In order to verify the accuracy of the results presented in this paper, we first compare our local work functions (cl>, = - eV;) with those measured by angle-resolved photoemission spectroscopy (ARPS)7and Kelvin probeforce microscopy (KPFM)1,1We note that sincethe accurate work function of the tip under the ambient conditions and also the accurate value of the dielectric constant for the N-LG/SiO2 interface are unknown, the difference of the work function is used to achieve more accurate comparison purposes. We begin by comparing  $\diamondsuit_1$  in a 4 · LG system with that measured by ARPS, as shown in Fig. 3(a). The results are given relative to the work function of the outermost layer <1>4 as the zero -reference level and  $Q_0$  is set to be 2.2 x 10<sup>13</sup> cm<sup>2</sup> It is evident from Fig. 3(a) that a very good agreement exists between the proposed discrete model and those measured by Ohta et al. 7. Another comparison study is conducted in Fig. 3(b) between the present discrete model and KPFM resultsof Ziegler et a/.11, who measured cl>, in the 1-6 - LG systems relative to that of bulkgraphitecl><sub>00</sub>. F i gure 3(b) clearly demonstrates that the measured work functions are generally in much better agreement with our results than those obtained by ab initio OFT calculations<sup>11</sup> when assuming a total induced charge density of 4.85 x 10<sup>12</sup> cm<sup>-2</sup>. We further perform a similar comparison in Fig. 3(c) between the present work functions at the uppermost layer of N-LG (cN) relative to those of (N-1)-LG (cN\_1) with KPFM results measured for N-LGwith layer number ranging from 1 to 8<sup>12</sup>. It is indicated that the present work functions closely match with the experimental observations for  $Q_0$  = 1.7 x  $10^{13}$  cm  $^{-2}$  .

Further comparison study is performed in Fig. 4 to investigate the influence of the effective mass  $m^{\bullet}$  on the charge distribution of an 8-LG system. It is seen from Fig. 4 that the model based on the monolayer-uke band structurefailsto accurately predict the charge distribution of the 8-LG system, in particular at the smaller induced charge densities. This figure also shows a significant deviation in the charge densities of layers  $i \ge 5$  for  $Q_0 = 10^{13}$  cm<sup>-2</sup>

Also, our energy evaluations of N-LG systems under a given  $Q_0$  for three possible charge distribution scenarios- (a) optimum distribution given in Eq. (3), (b) non-uniform distribution with the charge singularity at the very edge (i.e.,  $a_1 = 0$ ), and (c) fully uniform distribution (i.e.,  $q_1 = 0$ ) - reveal that the minimum energy is only achieved by the present optimum charge distribution model, further indicating its merit in predicting the charge distribution of other families of atomically thin layered materials.

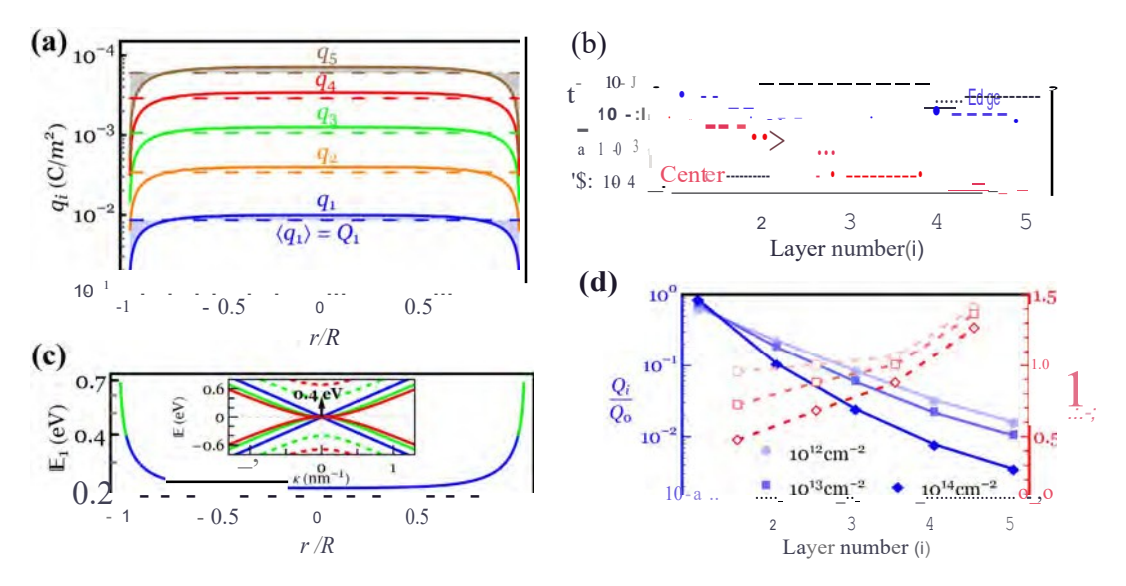


**Figure 5**. (a) Charge density profiles of a 5-LG system for  $Q_0 = 10^{13}$  cm  $^2$ , where each dashed line represents the average charge density (q;) = Q; in the layer i. (b) Charge density at the edgeq! and the center  $q_-$  of the layer i. (c) Fermilevel profile of the innermost layer. Inset:low-energy band structur of 5-LG system. Solid green curve in the Fermi level profile and dashed green curve in the band structure represent the first (0.4eV) excitation energy. (d) Blue cur ves: normalized average charge profiles across the layers of a 5-LG system for different gate charge densities of  $10^{12}$  (circles),  $10^{13}$  (rectangles) and  $10^{14}$  cm  $^2$  (diamonds). Red curves: corresponding changes in the local charge screening > ... u + i

La yer-by-Lay er ChargeDensity Profiles in 5-LG System. We now explore the unclear relationship between the total induced charge densities and the layer-by-layer charge density and Fermi level profiles. To this end, we begin by illustrating the charge density profiles of the 5-LG system when  $Q_0 = 10^{13} cm^{-2}$ , as shown in Fig. S(a) (see Fig. S2(a) in the SM for the corresponding Fermi level profiles). Consistent with the experiments of Ohta et al. 7 and Wang et al. 12, the charge density is drastically reduced as one move away from the innermost toward the outermost layer. However, the charge dens ity in the region very close to the edges is screened out an order of magnitude more weakly than that across the central region of the layer, as shown in Fig. S(b), which can be explained by the presence of the strong fringe field along the edges, as schematically shown in Fig. 1. Our results in Fig. S(a) also suggest that the innermost layer plays the most important role in the electrostatic charge distribution of the N-LG systems by hosting~70% of the gate charge density Q<sub>0</sub>. Hence, it is worth looking into its Fermi level profile more in detail, as illustrated in Fig. S(c). By following the evolution of the Fermi level along the innermost layer, it is observed that a strongcharge accumulation and thus sufficiently large shift in the Fermienergy at the edge can give rise to a jump in the electronic band structures of 5-LG toward the first excited state, 0.4eV (as shown in green solid curve in Fig. S(c) and in green dashed curve in the inset, which shows the energy band structure of the 5-LGsystem). However, our Fermi level analyses in the innermost layer of 6-and 8- LG systems exhibit few jumps in the Fermi level of the regions both close to and away from the edges when  $Q_0 = 10^{13}$  cm<sup>-2</sup> (see Fig. S2(b) of SM for detailed discussions). This can be attributed to the fact that the lowest energy of the first excitation band decreases for the N-LG system with a larger number of graphene layers, as shown in Fig. S(b).

To quantitatively elucidate the correlation between the magnitude of the gate charge density  $Q_0$  and the average charge distribution  $Q_i$  through the 5-LG thickness, Fig. S(d) shows  $Q_i|Q_0$  ratio as a function of the layer positions for three different values of  $Q_0$  (=  $10^{12}$ ,  $10^{13}$  and  $10^{14}$  cm  $^{-2}$ ). It is seen that a larger value of  $Q_0$  leads to a stronger charge screening normal to the layers, however, this effect dimin ishes when  $Q_0 < 10^{12}$  cm- $^{-2}$ . This figure also demonstrates that almost 90% of the excess charge density resides in the first two layers, implying that the interlayers creening length can reliably be determined to be less than  $\sim 0.7$  nm. Having  $Q_i$  data for each layer enables us to calculate the "local" (interlayer) charge screening > ..., f as  $Q_i + fQ_i = \exp(-df \setminus ..., f)$  based on Thomas-Fermi charge screening theory (seeSection S4 of SM for the calculation of the interlayer screening). It is deduced from Fig. 2(d) that the charge screening length between the first and second layers > ..., 2 may reduce from  $\sim$  Id at  $Q_0 = 10^{12}$  cm  $^2$  to  $\sim 0.5$  dat  $Q_0 = 10^{14}$  cm  $^2$ , while a smaller variation in > ..., + 1 is observed for the layers farther from the substrate due to the reduction in their DOS at the Fermilevel.

Layer-Dependent Charge Screening in N-LG Systems. We now turn to a discussion of the layer-dependent charge distribution/charge screening in 1-8-LG systems for a given gate-induced charge density of  $10^{13}$  cm<sup>2</sup>. Figure 6(a) presents a plot of Q;IQ, *versus*the layer positions in 1-8-LG systems, indicating that approximately 70%, 20%, 6% and 3% (99% overall) of Q<sub>0</sub> sit in layers i = 1 to 4, respectively, and thus the gate-induced electric field is not definitely felt by  $i \ge 4$  layers. Interestingly, we observed that the charge density of the layers located in the same position in N-LG systems decreases in a sawtooth-like fashion, as shown in the insets of Fig. 6(a) for the normalized charge density of the innermost Q/Q<sub>0</sub> and second innermost  $QifQ_0$  layers.

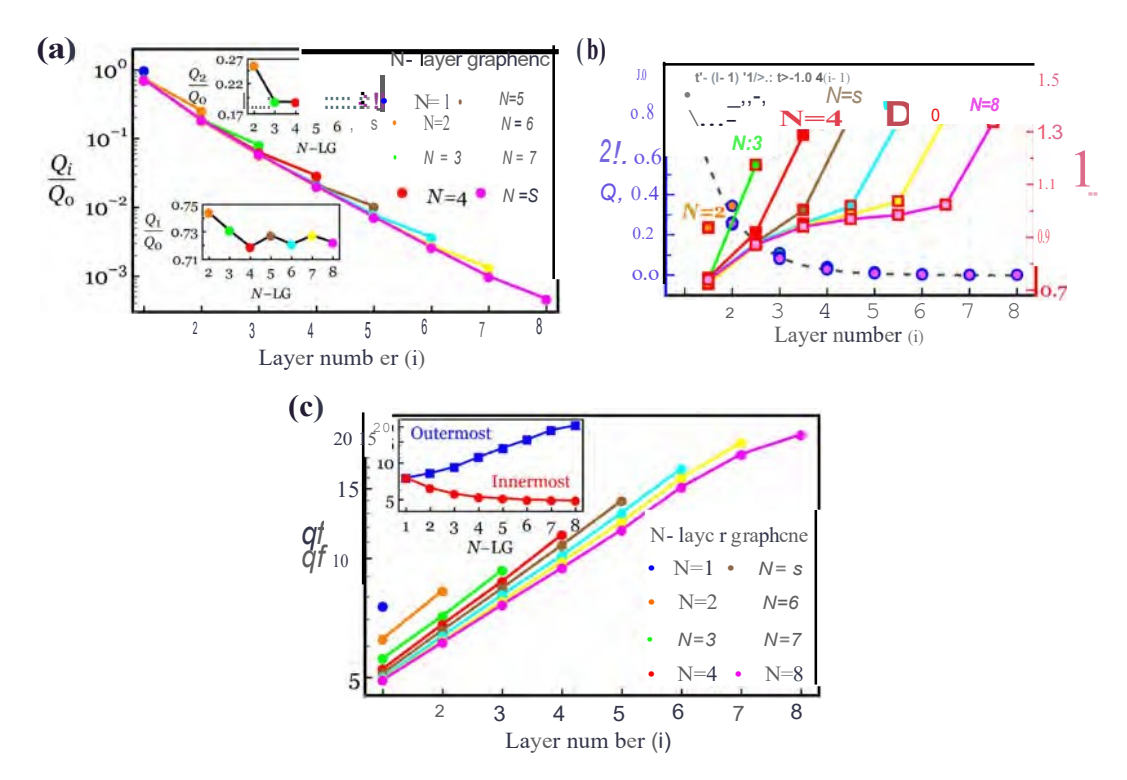


**Figure6.** (a) Normalized average charge distribution profilesacross the layers of 1-8-LG systems for  $Q_0 = 10^{13} \, \mathrm{cm}^{-2}$  Insets: Normalized charge density of the first (lower inset) and second (upper inset) layer in 2-8-LG. (b) Circles with blue borders: global charge screening length in 1-8-LG systems for  $Q_0 = 10^{13} \, \mathrm{cm}^{-2}$ . A decay length (d i > .) of 1.04 is found by fitting the data with a function  $c < i \rfloor \mathrm{JdA}$ , indicated by a dashed curve. Rectangles with red borders: local charge screening length in 1-8-LG systems for  $Q_0 = 10^{13} \, \mathrm{cm}^{-2}$ . (c) Edge-to-center charge density ratio as a function of the layer position in 1-8-LG systems when  $Q_0 = 10^{13} \, \mathrm{cm}^{-2}$ . Inset: Edge-to-center charge density ratio for the innermost (red circles) and outermost (blue squares) layers of 1-8-LG systems.

This saw-tooth pattern which is associated with the presence of the lin ear energy dispersion in N-LG with odd layer number has been experimentally confirmed through the measurement of the electric double-layer capacitance between an ionic liquid and 1-6-LG<sup>33</sup>. The results in Fig. 6(a) provide an important piece of information about the charge screening effect of the innermost layer on different layers of 2-8-LG. Hence, we first define a "global" (effective) charge screening >-. as Q;  $|Q_1| = \exp[-d(i-1)/>-.]$ . This new definition of the "global" charge screening length allows us to explore how the innermost layer impacts the surface potential drop across the FLG thickness and also provides a single value of the screening length to predict the charge distribution of all layers relative to that of the innermost layer. Keeping both global and local screening definitions in mind, we observe from Fig. 6(b) that our global charge screening can be well fitted by the simple exponential decay function (in particular for  $Q_0$ ;;  $10^{13}$  cm  $^2$ , see Fig. S3 of SM) when>-. iii., d. Figure 6(b) also illustrates the local charge screening between the adjacent layers of 1-8-LG, showing a much lower variation in >-.;;; +1 of the middle layers with an average value of -d, consistent with the global charge screening length. It is also observed from Fig. 6(b) that>-;; +ifd of the innermost and outermost interlayers becomes layer-independent for N? -1 and -1 and -1 are -1 and -1 and -1 are -1 and -1 are -1 and -1 and -1 are -1 and -1 and -1 are -1 and -1 ar

We next address the problem of the charge accumulation along the graphene edge, focusing first on very limited publications that have *quantitatively* studied the charge density at the edge of graphene thus far. From prior experimental work, a nearly th ree-fold increase in capacitance and thus the charge density near the edge of a suspended bilayer flake (0.4µm wide and 2.6µm long) was observed using quantum Hall edge channels²4. From theoretical pointsofview, the charge/dipole molecular dynamics model predicts a seven-fold (fifteen-fold) enhancement of the charge density at the edge (corner) over that at the center of a charged 8.5 nm x 4.8 nm rectangular graphene sheet²6 and a similar eight-fold enhancement of the chargedensity in a 20-nm-wide graphene nanoribbon²7. This model also suggests that the charge enhancement is more significant in multi-layered graphene in such a way that the chargedensity at the edge relative to that at the center can vary from 9 in the inner layer to > 14 in the outer layer of a 4-LG nanoribbon system²-7. Also, using the tight-binding Hartree model, the charge density along the edge of a 20-nm-wide graphene nanoribbon enhances up to five times over that at the center²8.

Having this quantitative description of the charge accumulation at the graphene edge in mind, we present in Fig. 6(c) the chargedensity at the edge relative to that at thecenter, q. •q. Q. As a function of the layer position in the 1-8-LG systems for  $Q_0 = 10^{13}$  cm- $^2$ As is evident from the figure, o discrete model predicts the edge-to-center charge density ratio for monolayer graphene to be  $\sim$ 7.5 which is consistent with the theoretical results  $^2$ 6- $^2$ 8. Surprisingly, the addition of each extra layer reduces the charge accumulation at the edge of the innermost layer from 7.5 in 1-LGdown to  $\sim$ 5 in 8-LG, whereas an inverse trend is observed for the charge accumulation at the

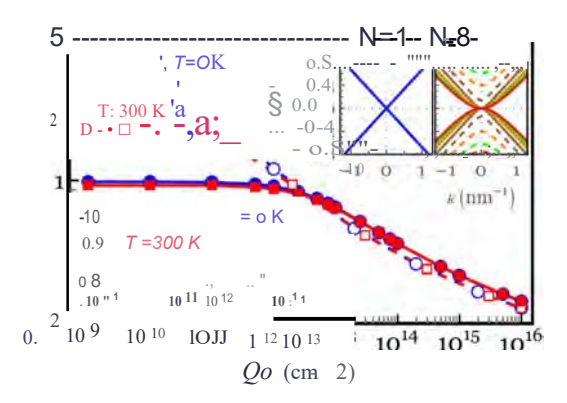


Figure 7. Local screening length between the first and second layers of an 8-LG system as a function of  $Q_0$ . Dashed curves with open circles (squares) represent the results obtained by the linear energy dispersion model (m = 0) at T = OK (T=300K), whereas solid curves with filled circles (squares) denote the results obtained by the actual energy dispersion of the 8-LG system  $(mj \times D)$  at T = OK (T = 300K).

edge of the outermost layer, whose value varies from 7.5 in 1-LG up to  $\sim$ 20 in 8-LG, as shown in the inset of Fig. 6(c). While the latter can be attributed to the presence of highly weak chargescreening at the edge due to the strong fringe field effect, as already shown in Fig. 5(b), the former may be accounted for by a combined effect of strong repulsive forces at the edge and the overall charge reduction in the innermost layer. It is worth pointing out that such reduction of the charge accumulation at the edge is observed in all other layers having the same position in the N-LG systems (for instance, see the second innermost layer in 2-8-LG) and the edge-to-center charge density ratio eventually converges to a constant value, showing nearly layer-independent behavior for N? 6.

Temperature-Dependent Charge Screening Model. While the present study has focused on the charge distribution of N-LG at absolute zero temperature, we note that a variation in temperature from zero to room temperature has no appreciable effect on the charge screening length, more specifically at the higher gate electric field. Following a tempera ture-dependent model of the charge distribution detailed in Section S5 of SM, the local chargescreening between the first and second layers of an 8-LG system is plotted in Fig. 7 as a function of  $Q_0$  at T=0 and 300K. For comparison purposes, the results of Kuroda et al. <sup>19</sup> based on the linear energy dispersion are reproduced bysettingmj = 0,as indicated bydashed curves with opensymbols in Fig. 7. It is evident from Fig. 7 that the interlayer charges creening is insensitive to the temperature variation when  $Q_0$ ? 5 x  $10^{12}$  cm and only a slight change in >.,.2 is observed at smaller gate charge densities (see lower inset) and ultimately saturates to > .1,2 d. Consistent with our temperature-independent charge screening length, Yang and Liu reported using the first-principles calculations that the interlayer screening, static perpendicular dielectric function and density of states of bi- and tri-layer graphene slightly changes as temperature increases from OK to 300 K to 600K34 It is also observed from Fig. 7 that the linear dispersion model fails to predict the interlayer charges creening between the two innermost layers for  $Q_0$  ::::  $10^2$  cm  $^2$  such that  $>_{1/2}$  goes to infinity (i.e.  $Q_2$  $Q_0$ -+ 0. Interestingly, a layer-by-layer inspection of the charge density in a similar 8-LGsystem for different values of  $Q_0$  reveals that the linear dispersion model not only yields inconsistent charge density profiles in almost all layers for  $Q_0$  ::;  $10^{12}$ cm  $^2$  but also shows a significant deviation in the charge densities of outer layers for  $Q_0 \ge 10^{12}$  cm<sup>-2</sup>, as shown earlier in Fig. 4. This deviation from our model can be understood in terms of the effective mass in N-LG with N? 2: an essential ingredient that is not captured in Kuroda's model where an N-LG system is considered as N parallel single layers with a massless linear energy dispersion (upper inset for N=1), rather than a single 2D system with the actual energy dispersion (upper inset for N=8).

# Conclusions

We developed a novel spatial discrete model to unravel the relationship between the macroscopic induced charge density and microscopic (layer-by-layer) charge distribution in finite-size FLG through considering the effects of both electrostatic interlayer screening and fringe field. We showed that adding each extra layer reduces the charge accumulation at the edge relative to that at the center of the innermost layer up to 20% (from ~7.5 in 1-LG down to ~5 in 8-LG). Our model offers a simple rule of thumb regarding the charge distribution in FLG: approximately 70%, 20%, 6% and 3% (99% overall) of the total induced charge density reside within the four innermost layers (layers i= 1 to 4, respectively), implying that the gate-induced electric field is not definitely felt by layers i > 4. We finally found that a variation in temperature from zero to 300K has no appreciable effect on the interlayer charge screening when the gate charge density is larger than  $\sim$ 5 x  $10^{12}$  cm  $^{-2}$  Although our study is concerned with FLG systems, the generality of our spatial discrete model suggests that the chargedensity profile, interlayer screening, quantum capacitance, and local surface potential of other atomically thin layered materials  $(ATLMs), such as semiconducting transition metal dichalcogenides (e.g., MoS_2, WSe_2 and WSi) and heterostructure and the semiconducting transition metal dichalcogenides (e.g., MoS_2, WSe_2 and WSi) and heterostructure (ATLMs), such as semiconducting transition metal dichalcogenides (e.g., MoS_2, WSe_2 and WSi) and heterostructure (ATLMs), such as semiconducting transition metal dichalcogenides (e.g., MoS_2, WSe_2 and WSi) and heterostructure (ATLMs), such as semiconducting transition metal dichalcogenides (e.g., MoS_2, WSe_2), and the semiconducting transition metal dichalcogenides (e.g., MoS_2, WSe_2), and the semiconducting transition metal dichalcogenides (e.g., MoS_2, WSe_2), and the semiconducting transition metal dichalcogenides (e.g., MoS_2, WSe_2), and the semiconducting transition metal dichalcogenides (e.g., MoS_2, WSe_2), and the semiconducting transition metal dichalcogenides (e.g., MoS_2, WSe_2), and the semiconducting transition metal dichalcogenides (e.g., MoS_2, WSe_2), and the semiconducting transition metal dichalcogenides (e.g., MoS_2, WSe_2), and the semiconducting transition metal dichalcogenides (e.g., MoS_2, WSe_2), and the semiconducting transition metal dichalcogenides (e.g., MoS_2, WSe_2), and the semiconducting transition metal dichalcogenides (e.g., MoS_2, WSe_2), and the semiconducting transition metal dichalcogenides (e.g., MoS_2, WSe_2), and the semiconducting transition metal dichalcogenides (e.g., MoS_2, WSe_2, W$ tures (e.g., graphene/MoS and MoSfWSe), can be characterized by feeding relevant electronic band structures of ATLMs into our model. In addition, the effect of structural defects (e.g., vacancies, adatoms, dislocations and grain boundaries) and stacking faults on the chargedistribution of defective FLG systems can be studied by modifying DOS of pristine FLG.

#### References

- Lee, C., Wei, X. D., Kysar, J. W & Hone, J. Measurement of the Elastic Properties and Intrinsic Strength of Monolayer Graphene. Science 321 (5887), 385-388 (2008).
- 2. Castro Neto, A. H., Guinea, F., Peres, N. M. R., Novose lov, K. S. & Geim, A. K. The Electronic Properties of Graphene. Rev. Mod. Phys. 8 1(1), 109 -162 (2009).
- 3. Nair, R. R., Blake, P., Grigorenko, A. N., Novoselov, K. S., Booth, T. J., Stauber, T., Peres, N. M. R. & Geim, A. K. Fine Structure Constant Defines Visual Transparency of Graphene. *Science* 320(5881), 1308-131S (2008).
- 4. Schwien, F. Graphene Transistors. Nature Nanotech 5(7),487-496 (2010).
- S. Bao, Q. & Loh, K. P. Graphene Photonics, Plasmonics, and Broadband Optoelectronic Devices. ACS Nano. 6(5), 3677-3694(2012).
- 6. Ostuji, T. et al. Graphene active plasmonics and their applications to terahertz lasers and sensors. Quantum Sensing and Nanophotonic Devices Xi, 8993 (2014).
- Ohta, T., Bostwick, A., McChesney, J. L., Seyller, T., Horn, K. & Rotenberg, E. Interlayer interaction and electronic screening in multilayer graphene investigated with angle-resolved photoemissions pectroscopy. *Phys. Rev. Lett.* 98, 206802 (2007).
- 8. Sun, D. et al. Spectroscopic Measurement of Interlayer Screening in Multilayer Epitaxial Graphene. Phys. Rev. Lett. 104, 136802 (2010).
- 9. Datta, S.S., Strachan, D.R., Mele, E.J. & Johnson, A.T.C. Surface Potentials and Layer Charge Distributions in Few-Layer Graphene Films. *Nano Lett.* **9(1)**, 7-11 (2009).
- Lee, N. J. et al. The interlayer screeningeffect of graphene sheets investigated by Kelvin probe force microscopy. Appl. Phys. Lett. 95, 222107 (2009).
- Ziegler, D., Gava, P., Giittinger, J., Molitor, F., Wirtz, L., Lazzeri, M., Saitta, A. M., Stemmer, A., Mauri, F. & Stampfer, C. Variations in the work function of doped single- and few-layer graphene assessed by Kelvin probe force microscopy and density functional theory. Phys. Rev. B83, 235434 (2011).
- Wang, X., Xu, J.B., Xie, W & Du, J. Quantitative Analysis of Graphene Doping by Organic Molecular Charge Transfer./. Phys. Chem. C. 115, 759676022011)
- 13. Ballestar, A., Esquinazi, P., Barzola-Quiquia, J., Dusari, S., Bern, F., da Silva, R.R. & Kopelevich, Y. Possible superconductivity in multi-layer-graphene by application of a gatevoltage. *Carbon*.72, 312-320 (2014).
- 14. Sui, Y. & Appenzeller, J. Scree ning and Interlayer Coupling in Multilayer Graphene Field-EffectTransistors. *Nano Lett.* 9(8), 2973-2977(2009).
- IS. Miyazaki, H., Odaka, S., Sato, T., Tanaka, S., Goto, H., Kanda, A. et al. Interlayer screening length to electric field in thin graphite film. Appl. Phys. Express I, 034007 (2008).
- Chen, H.A. Measurement of interlayer screeninglength of layered graphene by plasmonic nanostructure resonances. J. Phys. Chem. C.117, 22211-22217 (2013).
- 17. Visscher, P. B. & Falicov, L.M. Dielectric screen ing in a layered electron gas. Phys Rev B3, 2541-2547 (1971).
- 18. Guinea, F. Charge distribution and screening in layered graphene systems. Phys Rev B 75, 235433(2007).
- 19. Kuroda, M. A., Tersoff, J. & Martyna, G. J. Nonlinear screening in multilayer graphene systems. *Phys Rev Lett.* 106, 116804(2011).
- 20. Zimbovskaya, N. A. Specific featuresof electric charge screening in few-layer graphene films./ *Phys Condens Matter.* 25(4), 045302 (2013).
- 21. Goto, H., Uesugi, E., Eguchi, R., Fujiwara, A. & Kubozono, Y. Edge-depende nt transport properties in graphene. *Nano Lett.* 13, 1126-1130(2013).
- 22. Han, M. Y., Ozyilmaz, B., Zhang, Y. & Kim, P. Energy band-gap engineering of graphene nanoribbons. *Phys Rev Lett.* 98, 206805 (2007)
- 23. Chae, J. et al. Enhanced Carrier Transport along Edges of Graphene Devices. Nano Lett. 12(4), pp 1839-1844(2012).
- 24. Vera-Marun, I. J., Zomer, P.J., Veligura, A., Guimaraes, M. H. D., Visser, L., Tombros, N., van Elferen, H. J., Zeitler, U. & van Wees, B.J. Quantum Hall transport as a probe of capacitance profile at graphene edges. *Appl Phys Lett.* 102, 013106(2013).
- 25. Barraud, C., Cho T.,Butti, P., Shorubalko, I., Taniguchi, T., Watanabe, K.,Ihn, T. & Ensslin, K. Field Effect in the Quantum Hall Regime of a High Mobility Graphene Wire. *JApp/Phys.* 116, 073705 (2014).
- 26. Wilmes, A. A. R. & Pinho, S. T. A Coupled Mechanical-Charge/Dipole Molecular Dynamics Finite Element Method, with Multi-Scale Applications to the Design of Graphene Nano-Devices. *Int. J. Numer. Meth. Eng.* 100, 243-276 (2014).
- 27. Wang, Z. &Scharstein, R. W Electrostaticsof Graphene: Charge Distribution and Capacitance . *Chem Phys Lett.* 489, 229-236 (2010).
- 28. Andrijauskas, T., Shylau, A. A. & Zozoulenko, I. V. Thomas- Fermi and Poisson Modeling of Gate Electrostatics in Graphene Nanorihbon. *Lithuanian Journal of Physics* 52(1), 63-69 (2012).
- 29. Silvestrov, P. & Efetov, K. Charge accumulation at the boundaries of a graphene strip induced by a gate voltage: Electrostatic approach. *Phys. Rev. B* 77, 155436 (2008).
- 30. Vasko, F.T. & Zozoulenko, I. V. Conductivity of a Graphene Stripe: Width and Gate-Voltage Dependencies. *Appl. Phys. Lett.* 97, 092115(2010).
- 31. Thongrattanasiri, S., Silveiro, I. &de Abajo, F.J. G. Plasm ons in Electrostatically Doped Graphene. *Appl. Phys. Lett.* 100, 201105 (2012).
- 32. Berciaud, S., Potemski, M. & Faugeras, C. Probing Electronic Excitations in Mono- to Pentalayer Graphene by Micro Magneto-Raman Spectroscopy. *Nano Lett.* **14**,4548-4553(2014).
- 33. Goto, H., Uesugi, E., Eguchi, R. & Kubozono, Y. Parity Effects in Few-Layer Graphe ne. Nano Lett. 13, 5153 5158 (2013).
- 34. Yang, J.Y.&Liu, L. H. Effects of Interlayer Screening and Temperature on Dielectric Functions of Graphene by First-Principles. *I Appl Phys.* 120, 034305 (2016).

# Acknowledgements

This work was supported in part bythe National Science Foundation under Grant No. CMMI-1636132and in part bythe University of Michigan Rackham Predoctoral Fellowship.

### **Author Contributions**

H.R. and W.L. designed the study. H.R. developed the discrete model, carried out the calculations and analyzed the data. H.R. and W.L. contributed in the discussion and interpretation of the results. H.R. wrote the manuscript with input from W.L.

#### **Additional Information**

Supplementary information accompanies this paper at http://www.nature.com/srep

Competing financial interests: The authors declare no competing financial interests.

How to cite this article: Rokni, H. and Lu, W. Layer-by-LayerInsight into Electrostatic Charge Distribution of Few-Layer Graphene. *Sci. Rep.* 7, 42821; doi: 10. 10 38/srep4282 1 (2017).

Publisher's note: Springer Nature remains neutral with regard to jurisdictional claims in published maps and institutional affiliations.

institutional affiliations.

(a) Di This work is licensed undera Creative Commons Attribution 4.0 International License. The images

=a-1:11-- or other third party material in this article are included in the article's Creative Commons license, unless indicated otherwise in the credit line; if the material is not included under the Creative Commons license, users will need to obtain permission from the license holder to reproduce the material. To view a copy of this license, visit http://creativecommons.org/licenses/by/4.0/

© The Author(s) 2017